Proceedings of the 8th International Conference on Theoretical and Applied Nanoscience and Nanotechnology (TANN 2024)
Chestnut Conference Centre - University of Toronto, Toronto, Canada – June 10-12, 2024
Paper No. 103
DOI: 10.11159/tann24.103

Fluorinated Electrolyte for High-Voltage Lithium-Ion/Sulfur Chemistry with High Energy Density

Gebregziabher Brhane Berhe[a], Wei-Nien Su[b], Bing Joe Hwang[c]
[a] Adigrat University, Adigrat, Ethiopia,
[b, c] National Taiwan University of Science and Technology, Taipei, Taiwan
Conference center-University of Toronto, Toronto.ca

Abstract-*A new lithium-ion battery has been developed by combining a sulfurized carbon anode with a high voltage $LiNi_{0.5}Mn_{1.5}O_4$ (LNMO) cathode. The anode is derived from sulfurized polyacrylonitrile (SC(PAN)). When a traditional carbonate electrolyte with 1 M lithium hexafluorophosphate (LiPF6) is used, the capacity of the battery tends to decrease over time due to the decomposition of solvents. To solve this problem and enhance the compatibility of the S-C(PAN) and LNMO, the best electrolyte formulation for this new high-voltage lithium-ion battery consists of fluoroethylene carbonate (FEC), ethyl methyl carbonate (EMC), and 1, 1, 2, 2-Tetrafluoroethyl-2, 2, 3, 3-tetrafluoropropyl ether (TTE). These components are combined in a volume ratio of 3:2:5. When compared to the control electrolyte, the discharge capacity of the full cell made with 1 M lithium hexafluorophosphate (LiPF6) in FEC/EMC/TTE (3:2:5) electrolyte is 688 mAh g−1 at a rate of 2 C. X-ray photoelectron spectroscopy (XPS) results confirm that the fluorinated electrolyte effectively stabilizes both the S-C(PAN) and LNMO surfaces in the full cell.*

Keywords*:* Lithium-ion batteries, Fluorinated Electrolyte, Solid electrolyte interface, LNMO

1. Introduction

Energy storage is crucial in energy processes combined with renewable energy generations and lithium-ion batteries play a significant role in it.[1, 2] One way to increase energy and power density is by raising the operating voltage of lithium-ion batteries.[3] Moreover, to attain stable performance in terms of energy storage devices, a new battery system needs to be developed having a high capacity of anode material with high working potential cathode.[4, 5] Currently, researchers have developed and used some high-voltage cathodes materials such as $LiNi_{0.5}Mn_{1.5}O_4$ (LNMO), Li_2FeSiO_4, olivine-type $LiCoPO_4$, and layer-layer composite $xLi_2MnO_3(1\text{-}x)\ LiMO_2$ (M= Ni, Co, Mn).[6-8] However, using those high-voltage cathode materials has a critical problem and not yet commercialized. This is because of the severe oxidization decomposition electrolytes when the cell made with conventional carbonated based.[4] Nearly all of the electrolytes tend to decompose and high capacity fading originated from ethylene carbonate (EC) when the operating potentials are higher than 4.5 V vs Li/Li^+.[8-11] Consequently, developing stable high voltage lithium-ion batteries electrolytes for use with high voltage cathodes and anodes material will be critical. This means oxidation decomposition of the solvents in the electrolyte can be alleviated by developing a stable and high-voltage electrolyte solvents. A variety of strategies have been employed to address the unsatisfactory oxidation resistance of the conventional carbonate electrolytes. Some of them are a passivating layer on the surface of the positive electrode, surface medication, using super-concentrated electrolytes, and developing the inherent high voltage stability of electrolyte solvents. For example, novel solvents that have high oxidative potential, including sulfones, ionic liquids, and fluorinated solvents are hopeful to replace commercial carbonate solvents.[12-18]

Fluorinated solvents are more difficult to oxidize electrochemically due to high electronegativity and low polarizability of the fluorine atom. They have also a high flash point and lower melting point, which can improve safety and low-temperature performance, respectively. These are some of the advantages of fluorinated solvents relative to non-fluorinated solvents and considered as a promising candidate for high voltage lithium batteries electrolyte solvents.[19, 20] These fluorinated solvents will use in our system and study the compatibility of the electrolyte using the new electrochemical cell that contains sulfur composite anode and spinel high voltage cathode for lithium-ion batteries.

Lithium-ion//sulfur battery is an alternative cell configuration, the lithiation/delithiation reactions of high capacity sulfur composite materials take place at the anode side and transition metal oxide materials on the cathode side. The battery was

developed using intercalation cathode coupled to sulfur anode that would create a new system without lithium metal anode side (safety concern is reduced), based on the conversion reaction of sulfur species at the anode, and lithium-ion intercalation/de- intercalation at the cathode. The lithium-ion and electrons are generated by de-intercalate from the cathode while sulfur is reduced to form lithium sulfide (Li2S) by accepting lithium-ions and electrons.[21, 22] Therefore, Lithium-ion//sulfur cell can be potentially used as a powerful tool for developing high voltages electrolytes. Moreover, there is no studies reported so far (S-C(PAN)||LNMO) battery system.

Here, we systematical designed a cell by using S-C(PAN) as anode and LNMO as cathode for the first time. We introduced a new electrolyte composite of 1, 1, 2, 2-Tetrafluoroethyl-2, 2, 3, 3-tetrafluoropropyl ether (TTE), fluoroethylene carbonate (FEC), and ethyl methyl carbonate (EMC) with 1M LiPF6 as salt to study this high voltage lithium-ion battery. The optimized composition we found was FEC/EMC/TTE 3:2:5 v/v% (E2). The optimized electrolyte of FEC/EMC/TTE 3:2:5 shows enhanced Coulombic efficiency, rate capability and long term cycling stability of Li||S-C(PAN and Li||LNMO half-cells. More importantly, similar electrochemical enhancements are also obtained in the S-C(PAN)||LNMO full cell compared to carbonate electrolytes.

2. Experimental section

2.1. Synthesis of S-C(PAN) composite anode

The synthesis method and characterization of S-C(PAN) composite were reported in our previous study.[21] The elemental analysis determined the amount of sulfur content (44.74%) present in the S-C(PAN) composite. The specific capacity and sulfur loading during the electrochemical measurement of the half-cell and full-cell were calculated based on the sulfur content found in the S-C(PAN).

2.2. Electrolytes preparation and electrodes

All lithium battery-grade was obtained from Sigma Aldrich. The commercial electrolyte 1M lithium hexafluorophosphate (LiPF6) electrolyte in a mixture of ethylene carbonate (EC) and diethylene carbonate (DEC) (1:1 v/v %, 99%) as-received was used as a base electrolyte (termed as BE). Fluoroethylene carbonate solvent (FEC, 99.9%), 1, 1, 2, 2-tetrafluoroethyl-2, 2, 3, 3-tetrafluoropropyl ether (TTE, 99.9%) and ethyl metal carbonate (EMC, 99.9%). The solvents were treated with 10 wt % of a 3 Å molecular sieve for 3 days to remove trace moisture impurities before use. 1 M LiPF6 dissolved in FEC and TTE at a weight ratio of 3:7 v/v% was used (termed as E0). 1M LiPF6 electrolyte was prepared by using a calculated amount of LiPF6 dissolved first in (FEC) and mixed with EMC. Finally, TTE was added into the prepared solution. The EMC-containing electrolyte was 1 M LiPF6 in 3:2:5 v/v% FEC/EMC/TTE (termed as E2). All electrolytes were prepared in an Ar-filled glove box with oxygen and moisture contents below 0.1 ppm and the salt was dried at 80 °C in an evacuated oven in a glove box.

The negative electrode was prepared by using S-C(PAN), sodium carboxymethyl cellulose (CMC) binder, and Super P in a weight ratio of 80:10:10, respectively. The solvent was prepared by mixing ethanol and water (1:1 wt%). The binder (CMC) was dissolved in the prepared solvents with continuous stirring for the whole three days at room temperature. The active material and super P were grinding them together and dispersed in the prepared binder solution. The prepared slurry was coated onto Al foil current collector using doctor blade and vacuum- dried at 60 ^{o}C for 12 h. The electrode laminates were roll-pressed and punched into electrode discs (13 mm diameter). The sulfur loading in the S-C(PAN) electrode and capacity of the anode to cathode ratio (A/C) were 1.15 mg cm^{-2} and 0.93, respectively. The current density of the half-cell (Li||S-C(PAN) and full-cell (S-C(PAN)||LNMO) were calculated based on the sulfur for all electrochemical tests. The loading density of LNMO electrode was 13 mg cm^{-2} and obtained from Aleees (Advanced Lithium Electrochemistry Co.,Ltd, Taiwan). The proportion positive electrode is 90:5:5 (LNMO: Supper P: polyvinylidene fluoride, PVDF). The positive electrode is punched into discs and further dried at 70 °C under vacuum overnight.

2.3 Electrochemical measurement

2032 type coin cells were assembled (both half and full-cells) in an argon-filled glove box (UNIlab Plus Glove Box, MBraun), where oxygen and moisture levels less than 1 ppm. For all electrochemical measurements a

PP/PE/PP composition (Celgard 2325) separator, the type was placed between the anode and cathode, and the different electrolyte was used for each cell. The galvanostatic charge-discharge tests of Li||LNMO and discharge-charge of Li||S-C(PAN) were performed using a computer-controlled battery tester (Arbin BT-2000) within a potential range of 1.0−3.0 and 3.0-5.0 V for cell, respectively. The full cell (S-C(PAN)||LNMO) was assembled by S-C(PAN) used as negative and LNMO as the positive electrode and it tested between 1.0-3.7 V. Sixty (60) µl amount of electrolyte was used in this work. Electrochemical impedance spectroscopy (EIS) was performed for the half and full-cells within a frequency range of 0.01Hz to 100 kHz at a potential amplitude of 10 mV using an impedance analyzer (BioLogic SAS) after different cycles using coin cells. EIS measurements were performed after a full discharge state. Cyclic voltammetry (CV) scans were performed by using VMP3 multichannel (BioLogic Science Instruments work station) at a scan rate of 0.1 mV s^{-1}, between 1.0-3.7 V for the (S-C(PAN)||LNMO) system.

2.4 Material characterization and measurements

The ball milling machine or E $_{max}$ (Retsch GmbH, Allee, 42781 Haan, 2600W) with grinding jar size of 125 ml was used for grinding the mixture of sulfur and PAN having Zirconia balls of 5 mm. The sulfur content in composite (S-C(PAN)) was determined by elemental Vario EL cube (for NCSH, German) analyzer using a thermal conductivity detector. The ionic conductivities of the electrolyte were measured from the EIS spectra, which abstained by assembling symmetric cells using two stainless steel electrodes at room temperature (25 ^{o}C). For SEM and XPS, both (S-C(PAN) and LNMO) were collected by disassembling the cells inside the glove box after the desired cycle and washed with DEC until all the residuals were removed and dried in vacuum for 24 h at 80 °C before analysis. The surface morphology of the cycled electrodes was evaluated by Field emission scanning electron microscopy (JEOL JSM- 6500F) with an accelerating voltage of 15 kV after fully discharged. The surface of both S-C(PAN) and LNMO was examined when the cell performed at the half and full-cells. Further, X-ray photoelectron spectroscopy (XPS, PHI, 1600S) was used to analyze the chemical composition of the electrode surface in the full-cells at NSRRC using 0.05 eV step and 20 eV pass energy. It was calibrated by gold signal at a binding energy of 84.0 eV.

3. Result and discussion

The **physicochemical properties of electrolytes** were studies by using viscosity and conductivity. The Lovis dynamic viscosity of the different electrolytes is given in Table S1. The Lovis dynamic viscosity of E0 and E2 is 0.672 and 0.096 mPa·s, respectively, indicates that enhanced the fluidity of the electrolyte. The reason for the low viscosity of E2 compared to E0 is due to the addition of EMC solvents. The ionic conductivity of BE, E0, and E2 electrolytes was measured via EIS using symmetric cells with two stainless steel electrodes. Figure S1 shows the impedance spectra of the difference for the electrolytes of BE, E0, and E2. The bulk electrolyte resistance (R) was used to calculate the ionic conductivity based on the following formula:

$$R = \rho \frac{l}{A}$$

Where ρ is resistivity (Ω*cm), A is a cross-sectional area (cm^2), l is the distance between two electrodes (cm), R represents the resistance of the electrolyte solution (Ω). The ionic conductivity (κ) of the electrolyte is the reciprocal of the resistivity (ρ). As can be seen from Table S2, the calculated ionic conductivity of the different electrolytes is 0.4713, 0.1592, and 0.3792 S cm^{-1} BE, E0, and E2, respectively and it is ascribed to the high viscosity of FEC and TTE.

Electrochemical measurements and characterizations: The electrochemical suitability of F-containing electrolyte was investigated with both half-cells (Li||S-C(PAN) and Li||LNMO) and full-cell (S-C(PAN)||LNMO). The capacity of the anode to cathode (A/C) ratio of the full-cell was rational design based on the practical capacity values of the

half-cells. The cycling performance and rate capability of Li||LNMO was measured at a 0.3 C-rate cycled between 3.0–5.0 V. Figure 1a compares the first charge-discharge curves of LNMO cathode at 0.3 C-rate uses BE and the two F-containing electrolytes. As can be seen from the first cycle, the inial discharge capacity of E2 shows a greater and higher reversible capacity of 139 mAh g^{-1} and displays a relatively enhanced initial Coulombic efficiency of 93.9% compares to BE having a discharge capacity of 131 mAh g^{-1} with initial Coulombic efficiency of 91.78%. The fluorinated electrolytes contribute to the Coulombic efficiency and capacity of the cell. Figure 1b compares the cycling performance of Li||LNMO half-cells cycled using the various electrolytes. The retention capacity of LNMO cathode cycled at 0.3 C-rate using BE, E0, and E2 is 46.7, 49.3, and 73.6%, respectively. The control electrolyte (BE) shows low capacity retention and it is due to oxidation decomposition at the high operating voltage.[9] In contrast, the cell assembled using fluorinated electrolytes exhibits a highly reversible capacity and showing superior cycling stability at high voltage battery. Especially E2 showing the best cycling stability due to low viscosity and high conductivity compared to other fluorinated electrolytes (E0), which could attribute low interfacial impendence of the electrode as will be discussed later. Figure 1 C-rate shows the rate capability of Li||LNMO using various electrolytes using different C-rates. The main reason for the lower discharge capacity difference of E2 relative to BE is due to serious electrolyte decomposition and reduced Coulombic efficiency. The discharge capacity of the cell at 1 C is 102.04, 86.34, and 110.77 mAh g^{-1} for BE, E0, and E2, respectively. E2 shows higher discharge capacity and stable rate capability of all cells. These data suggest that fluorinated electrolyte having a high conductivity of the electrolyte solution and improves the rate performance of high voltage cells.

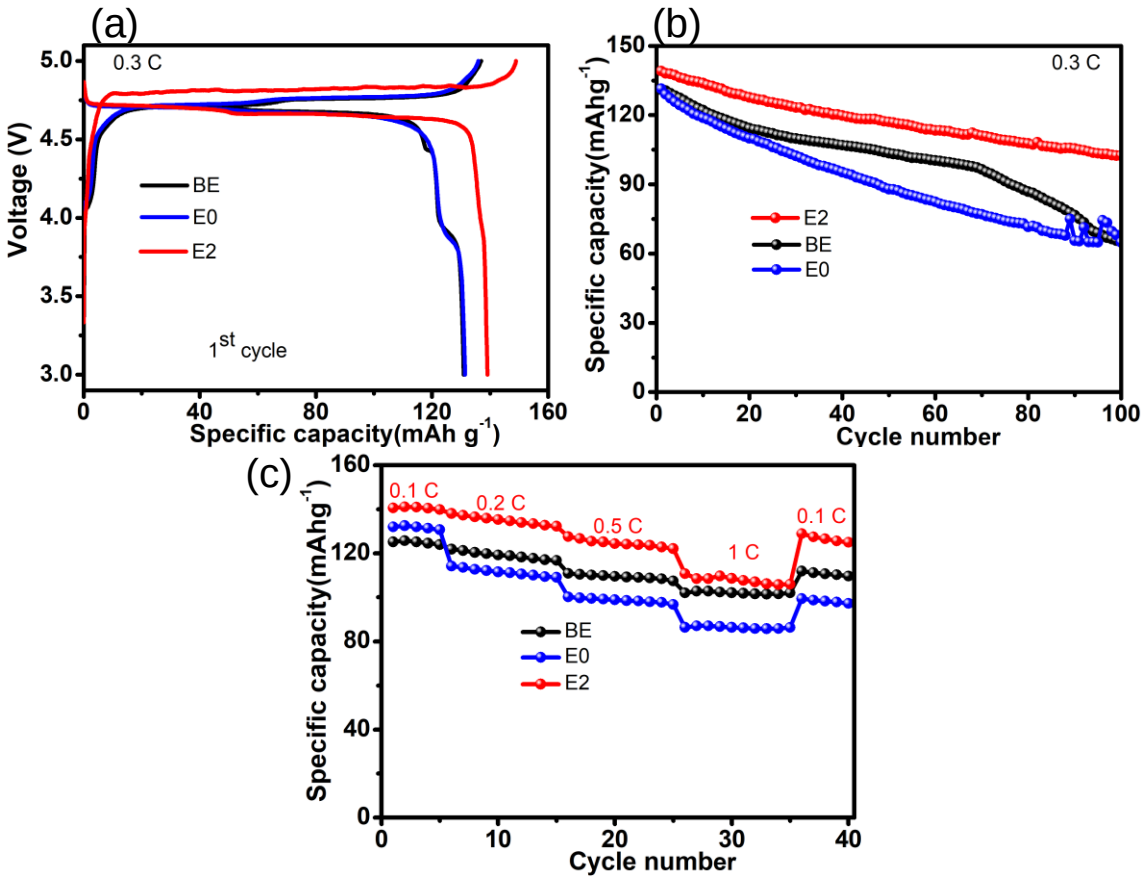

Fig. 1. Electrochemical performance of Li||LNMO half-cell at various electrolyte: (a) Initial charge /discharge curve of the cell at 0.3 C-rate, (b) cycling performance over 100 cycles at 0.3 C-rate, and (c) Rate performances measured at various C-rates, which were the same for both charge/discharge in each cycle.

The discharge-charge curves of S-C(PAN) electrode in carbonate and fluorinated based electrolyte are presented in Figure 2. The initial discharge-charge of S-C(PAN) anode cycled at 0.3 C-rate within the potential range of 1.0-3.0 V using various electrolytes is given in Figure 2a. Essentially, no significant variation in the initial capacity and Coulombic efficiency of the various electrolytes performed Li||S-C(PAN). The reversible discharge capacity of Li||S-C(PAN) using E2 electrolyte is 1430 mAh g^{-1} with the first Coulombic efficiency 79% and shows excellent cycling stability with a reversible capacity of 1399 mAh g^{-1} after the 150th cycles at 0.3 C rate. Besides, the reversible capacity retention of the cell is 97.86% after 150 cycles as shown in Figure 2b and it exhibits a corresponding low capacity fading rate of 0. 014% per cycle. Furthermore, the reversible capacity retention (capacity decay rates in parentheses) of BE and E0 is 57.12% (0.28% per cycle) and 8.65% (0.91% per cycle) after 150 and 100 cycles at 0.3 C rate, respectively as presented in Figure 2b. The retention capacity of Li||S-C(PAN) cell was calculated from its second cycle. The cell cycled with E2 electrolyte shows better cycling performance relative to a non-fluorinated electrolyte, due to the formation stable SEI layer of the sulfur composite by reductive decomposition of fluorinated solvents. In addition, the lithium anode forms a protective layer that acts as physical barriers to eliminate undesirable side reactions. In contrast, the electrochemical performance of the cell cycled using E0 electrolyte shows a high capacity fading due to its high viscosity and it may also due to the incompatibility of the electrolyte to lithium anode. The film formed using this electrolyte is not good enough to suppress undesirable side reactions. The rate capability of Li||S-C(PAN) half-cell in the electrolyte having different compositions are presented in Figure 2c. The rate performance of S-C(PAN) electrode in the BE and E0 somewhat worse than the EMC containing electrolyte (E2) when the cell cycled greater than 0.5 C-rate. This is due to the high ionic conductivity of E2 compared to E0, like what we discussed in the rate capability of Li||LNMO. In another hand, fluorinated electrolyte exhibits better rate capability by forming conductive SEI on the sulfur composite cathode. Furthermore, the initial discharge capacity of the cell cycled at 2 C-rate is 709, 69, and 1007 mAh g^{-1} for BE, E0, and E2 respectively, and E2 shows the highest discharge capacity as depicted in Figure 2c.

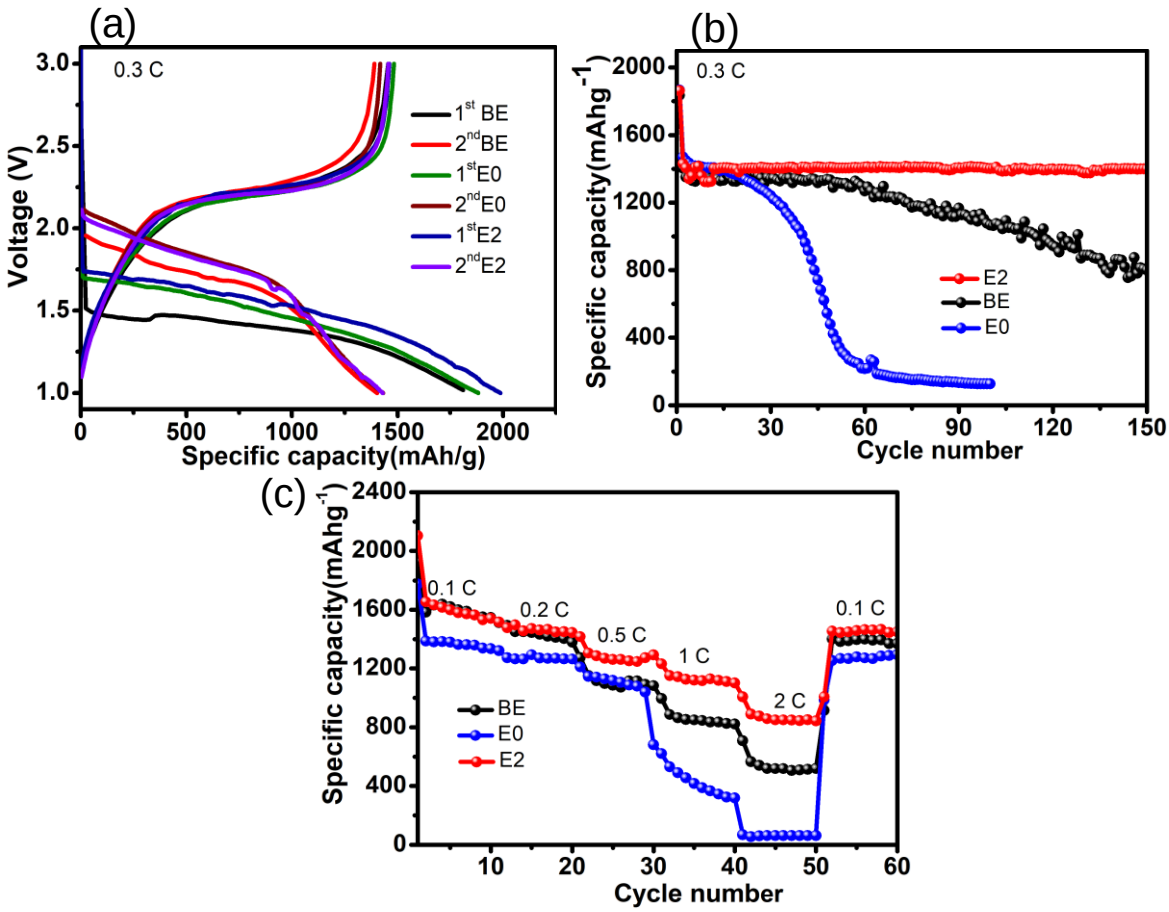

Fig. 2. Electrochemical performance of Li||S-C(PAN) half-cell at various electrolyte: (a) Initial charge/discharge curve of the cell at 0.3 C-rate, (b) cycling performance over 150 cycles at 0.3 C-rate, and (c) Rate performances measured at various C-rates, which were the same for both charge/discharge in each cycle.

The effect of newly developed high-voltage, cost-effective systems capable of Fluorine-based electrolytes has also investigated by using the new demonstrated high voltage system. Full-cell (S-C(PAN)||LNMO) assembled as a tool to study the various electrolytes for the first time with a potential range of 1.0-3.7 V. The A/C ratio is calculated from the capacity of the half-cells (Li||S-C(PAN) and Li||LNMO). The initial charge-discharge curves of the S-C(PAN)||LNMO full cells cycled using BE, E0, and E2 are shown in Figure 3. The initial discharge capacity cells made with BE, E0, and E2 electrolytes are 1084, 1060, and 1094 mAh g^{-1} at 0.4 C-rate, respectively as depicted in Figure 3a. Figure 3b shows the retention capacity of a cell cycled with E2 electrolytes is 73% after 100 cycles. In addition, the reversible capacity retention of BE and E0 is 15.49% and 65.28% after 100 cycles at 0.4 C rate, respectively. The capacity fading of the full-cell made with E0 and E2 significantly reduced and stable electrochemical performance was achieved.The high resistance was built up at the electrode interface caused by the deposit of organic decomposition BE electrolytes and that is the reason for the fast capacity fading. On the other hand, the fluorine rich electrolytes proved a good passivation layer formed on the electrode/electrolyte interface by the reductive decomposition of fluorinated solvents formed SEI on the anode side, togather with CEI on the cathode. Finally, E2 is the optimized electrolyte as seen from both half and full-cells electrochemical performance results. Figure 3c compares the rate capability of the full-cells cell with carbonated (BE) and fluorinated (E2) electrolytes. The discharge capacity of the cell made with E2 electrolyte is 688 mAh g^{-1} a rate of 2 C, which is significantly higher than the 19 mAh g^{-1} for the cell with BE electrolyte. The best rate performance of cells with E2 electrolyte is due to the formation of the

conductive film formed at the interface. Figure 3d compares also the cyclic voltammogram (CV) of full cell measurements that were performed with BE and E2 electrolyte with the potential range of 1.0-3.7 V 0.1 mV s^{-1}. The peak appeared at 3.36 V positive scan whereas a negative scan appears at 2.37 V. The cell cycled using fluorinated electrolytes (E2) has a more pronounced peak than BE, indicating that due to the formation of good film from reduction decomposition of FEC and TTE contributes to the formation of CEI on the cathode side.

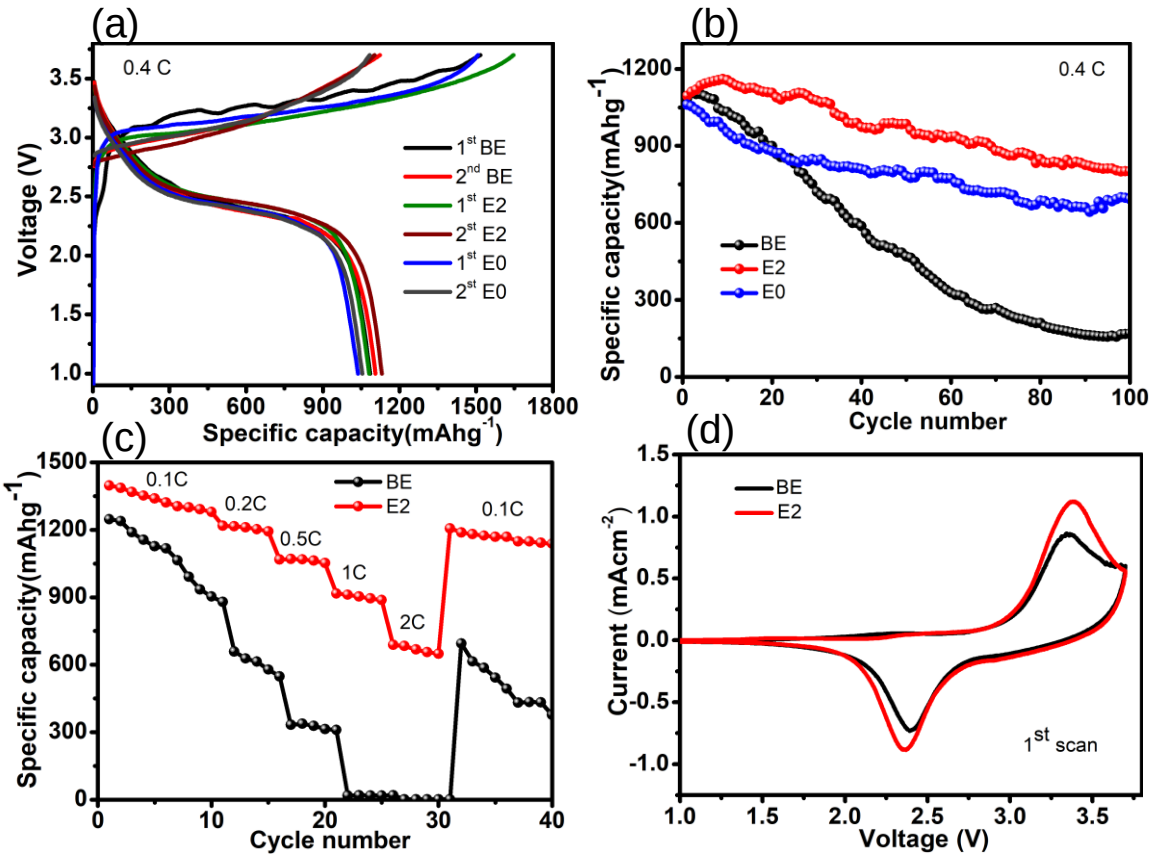

Fig. 3. Electrochemical performance of S-C(PAN)||LNMO full cells at various electrolyte within a poetical range of 1.0–3.7 V: (a) initial charge /discharge curve of the cell at 0.4 C-rate, (b) cycling performance over 100 cycles at 0.4 C-rate, (c) Rate performances with BE and E2 electrolytes, and (d) cyclic voltammograms of S-C(PAN)||LNMO full-cell at the initial scan within the voltage range of 1.0–3.7 V at a scan rate of 0.1 mV/s.

X-ray photoelectron spectroscopy (XPS) is utilized to elucidate the chemical composition of both S-C(PAN) anode and LNMO cathode in the full cell cycled using BE and E2 electrolytes. XPS spectra of F-1s and Li-1s of the cycled S-C(PAN) anode with two electrolytes in the full-cells are presented in Figure 4. The Li-1s spectra of cycled S-C(PAN) anode in the full-cells, after 50 cycles at 0.4 C in a complete discharge state using BE and E2 electrolytes are depicted in Figure 4a, and 4c, respectively. The peaks at 55.7 eV in Li-1s spectra are attributed to LiF respectively.[23, 24] The peaks appeared from 52-54 eV, may be assigned to the Li atoms in an oxide environment such as Li_2O.[25]

Likewise, the peaks at 684.8, 687, and 688.4 eV in the F-1s spectra cycled displayed in Figure 4b can be assigned to LiF, $Li_xPO_yF_z$, and C-F_3, respectively. Furthermore, Figure 4d also displayed two pronounced peaks at 684.8 (LiF) and 686.7 eV (semi-ironic C-F_2).[26-29] The pronounced peaks and mainly composed of inorganic LiF is formed in E2 electrolyte in both Li-1s and F-1s spectra. This indicates that the formation of stable SEI after the first cycle is due to the presence of fluorine-rich species which passivate the anode surface. Moreover, the presence of LiF in SEI composition is due to fluorine-containing species in the interfacial decomposition reaction. In contrast, the lower peak intensity of LiF formed when the

cell made using BE electrolyte indicates that the SEI is mainly derived solvent decomposition and it agrees well with the higher capacity fading of the full cells.

Similarly, to investigate the CEI layer components in the full-cell, the cycled LNMO electrodes were examined by XPS after 50 cycles using 0.4 C-rate. Figure S2 shows the XPS spectra of the Li-1s and F-1s peaks on the LNMO cathode cycled using BE and E2. The Li-1s spectra of LiF (55.7 eV), $ROCO_2Li$ (54.5 eV), and Li_2O are presented in Figure S2a and S2c. The peaks at 684.8 and 686 eV correspond to LiF and C-F, respectively, as shown in Figure S2b and S2d.[24] However, there are some peaks at 682.6 eV for F-1s spectra (Figure S2a and S2b) assembled the cell with BE and E2 are not clearly assigned to a particular compound or functional groups. The LiF peak for the cell made with BE has a relatively weak intensity and dominated by organic compositions as shown in Figure S2a and S2b. In contrast, the cell assembled with E2 electrolytes has a quite strong peak intensity and a more highly LiF dominated CEI composition. It reveals that the TTE participates or contributes to the formation of CEI formation on the LNMO cathode side.

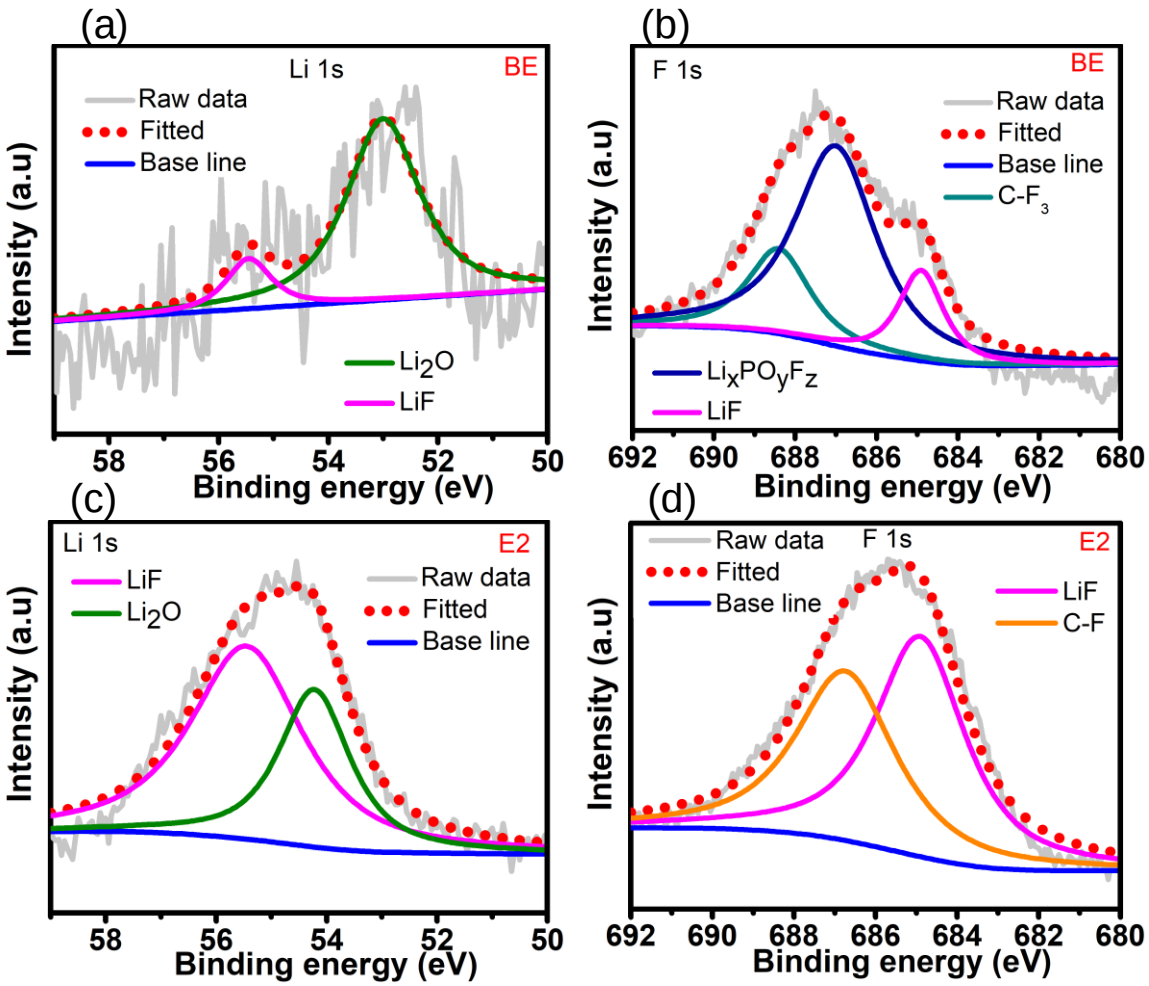

Fig. 4. XPS spectra of anode electrode used for S-C(PAN)||LNMO full cells cycled using different electrolyte: (a) Li-1s spectra cycled using BE, (b) F-1s spectra cycled using BE, (c) Li-1s spectra cycled using E2, and (b) F-1s spectra cycled using E2.

EIS of Li||LNMO, Li||S-C(PAN), and S-C(PAN)||LNMO was measured to examine the possible reason for enhanced performance cell made with fluorinated relative to the carbonate electrolytes. Figure 5 shows the EIS spectra of all cells measured with all electrolytes after the 50 cycles (both half-cells) and 100 cycles (full-cells). Figure 5a compares the Nyquist

plots of Li||LNMO half-cells cycled with all electrolytes. The cells have one semicircle in the high frequencies regions and it ascribed to the Li^+ diffusion through the SEI on the surface of the electrode. As can be observed from Figure 5a, the resistance of the cell with E0 electrolyte was very high, which suggests that due to lower conductivity. Moreover, the higher resistance of the cell made with E0 electrolytes due to the incompatibility/side reaction of electrolyte solvents and Li^+ to that anode that deteriorates the electron and ion diffusion within the anode matrix. Besides, the higher interfacial resistance BE electrolyte is due to a thick film layer formed as the results of electrolyte decomposition at high voltages.[30] In contrast, the cell made with fluorinated electrolyte (E2) exhibits obviously lower resistance. This is due to the higher oxidation stability of the cell and which indicates the formation of an ionic conductive film, that stabilizes the electrode surface. Figure 5b compares also the Nyquist plots of Li||S-C(PAN) half-cells with all electrolytes. The resistance of the cell cycled using E2 electrolytes is lower than that of the cell with and without fluorinated solvents. The resistance is effectively suppressed by the addition of EMC solvents , such clear impedance difference is due to high ionic conductivity of the electrolyte and formation of stable and conductive SEI on the sulfur cathode. Finally, the Nyquist plots of the full cells cycled using all electrolytes compared as shown in Figure 5c. The interfacial resistance of the fluorinated electrolyte (E0 and E2) cell shows a significantly lower compared to the carbonate-based electrolyte, suggesting that fluorine-based electrolyte efficiently suppressed electrolyte decomposition on the surface electrodes, is also good agreement with cycling performance of the full-cells results. The lower interfacial resistance of the full cell at the electrode/electrolyte interface indicates the formation of an ionic conductive at the interface.

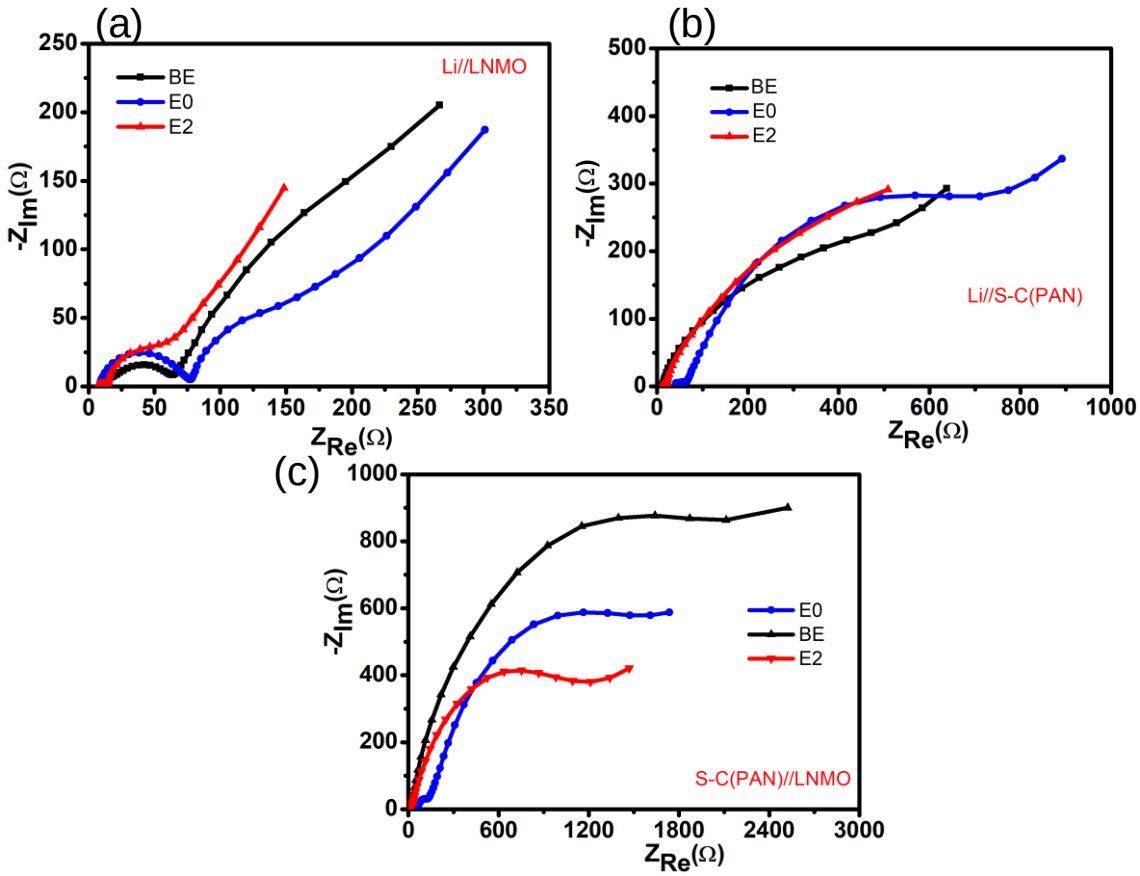

Fig. 5. Comparison of EIS measurements for different electrolytes within half and full-cells: (a) Li||LNMO, (b) Li||S-C(PAN), and (c) S-C(PAN)||LNMO in the frequency range of 100 kHz and 0.01 Hz with a perturbation amplitude of 10 mV.

Morphological analyses of the full cells: SEM image of the full-cells was carried out after 100 cycles to see the surface morphology of LNMO and S-C(PAN), cycled with fluorine (E0 and E2) and carbonated-based (BE) electrolytes as shown in Figure 6 and Figure S3. Figure 6a and 6c are the SEM images of LNMO cathodes cycled with BE and E2 electrolytes, respectively. For the BE electrolyte cell, the thick and rough surface was observed, which is due to heavy decomposition products deposited. In contrast, for the E2 electrolytes cel, the surface morphology of the LNMO cathode appears to be quite smooth and clean surface, suggesting that an effective passivation layer formed by the fluorine-based electrolytes. Figure S3a also shows relatively better morphology than the cell made with BE. As shown in Figures 6b, the SEM image of the S-C(PAN) electrode cycled BE electrolytes shows a not good and crack surface whereas the surface of the electrode cycled using fluorinated electrolytes (E2) exhibits quite smooth with a clean surface (Figure 4d). This suggesting that, a fluorine-based suppressed electrolyte decomposition and reduced the side reactions at the interface. Even though the surface morphology of S-C(PAN) cycled with E0 is better than BE, its surface is as not smooth as that of E2 as depicted in Figure S3a.

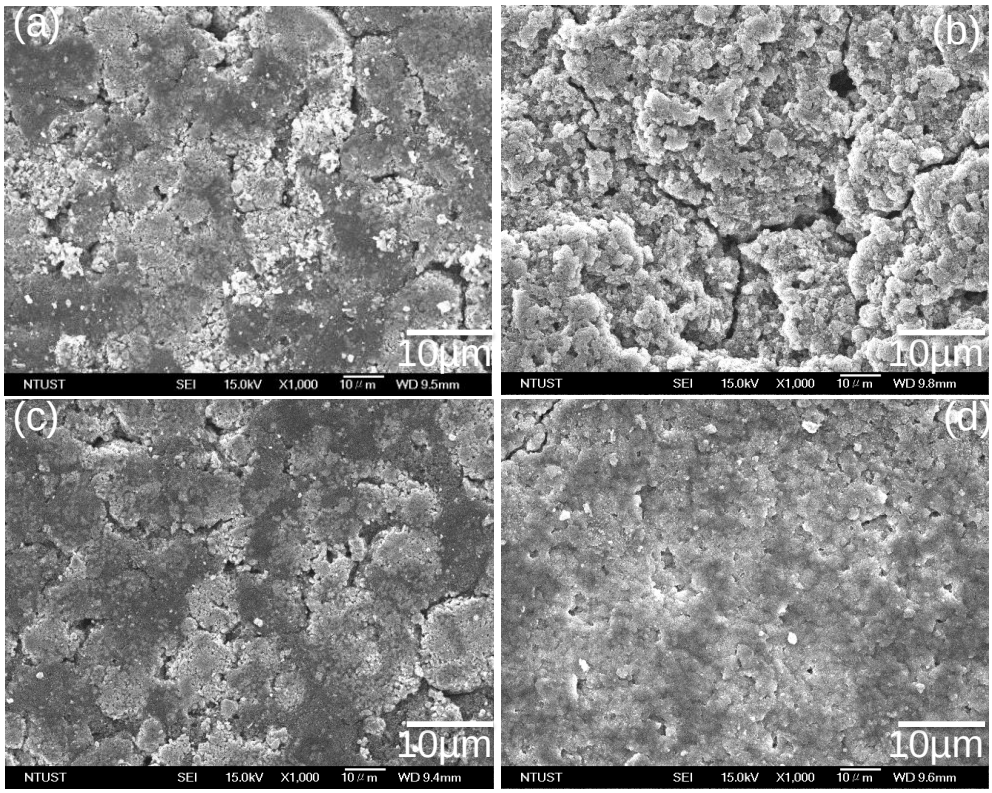

Fig. 6. SEM images of the electrode in the full-cell: (a) LNMO cathode cycled with BE, (b) S-C(PAN) anode cycled with BE, (c) LNMO cathode cycled with E2, and (d) S-C(PAN) anode cycled with E2.

4. Conclusion

In conclusion, we have systematically designed a new cell by coupling S-C(PAN) as anode with LNMO cathode for the first time and it uses as a tool developed electrolytes. A high-voltage electrolyte composed of FEC/EMC/TTE (3:2:5) has been developed. The addition of EMC to the electrolyte solution reduced the viscosity, as a result, it increased the ionic conductivity. The optimized electrolyte improvs Coulombic efficiency, rate capability, and long term cycling stability of both half-cells (Li||S-C(PAN and Li||LNMO) and full-cells S-C(PAN)||LNMO full cell were achieved. Good passivating capability and oxidative durability at high-voltage of the full-cell is also observed from CV measurements. The XPS studies show that inorganic LiF rich SEI on the developed on the S-C(PAN) anode. Moreover, The CEI developed on the LNMO

cathode suppresses irreversible degradation in the high-voltage. The high cycling stability and long durability are due to the formations of fluorine rich layers formed between the electrode/electrolyte interfaces.

Conflicts of interest

There is no conflict of interest to declare.

Acknowledgments

Financial support from the Ministry of Science and Technology (MoST) (106-2923-E-011-005, 105-3113-E-011-001, 105-ET-E-011-004-ET, 104-2923-M-011-002-MY3, 104-2911-1-011-505-MY2, 103-2221-E-011-156-MY3), the Ministry of Economic Affairs (MoEA) (101-EC-17-A-08-S1-183), the Top University Projects (100H45140), the Global Networking Talent 3.0 Plan (NTUST 104DI005) from the Ministry of Education of Taiwan, and Taiwan's Deep Decarbonization Pathways toward a Sustainable Society Project (AS-KPQ-106- DDPP) from Academia Sinica, as well as the facilities of support from the National Taiwan University of Science and Technology (NTUST) and National Synchrotron Radiation Research Centre (NSRRC), are acknowledged.

Reference

[1] B. Zhu, X. Wang, P. Yao, J. Li, J. Zhu, Chemical Science, (2019).
[2] A.M. Tripathi, W.-N. Su, B.J. Hwang, Chemical Society Reviews, 47 (2018) 736-851.
[3] S. Tan, Y.J. Ji, Z.R. Zhang, Y. Yang, ChemPhysChem, 15 (2014) 1956-1969.
[4] X. Zheng, Y. Liao, Z. Zhang, J. Zhu, F. Ren, H. He, Y. Xiang, Y. Zheng, Y. Yang, Journal of Energy Chemistry, 42 (2020) 62-70.
[5] H. Kawasoko, S. Shiraki, T. Suzuki, R. Shimizu, T. Hitosugi, ACS Appl Mater Interfaces, 10 (2018) 27498-27502.
[6] M. He, C.C. Su, Z. Feng, L. Zeng, T. Wu, M.J. Bedzyk, P. Fenter, Y. Wang, Z. Zhang, Advanced Energy Materials, 7 (2017) 1700109.
[7] L. Chen, X. Fan, E. Hu, X. Ji, J. Chen, S. Hou, T. Deng, J. Li, D. Su, X. Yang, C. Wang, Chem, 5 (2019) 896-912.
[8] L. Xia, L. Yu, D. Hu, G.Z. Chen, Materials Chemistry Frontiers, 1 (2017) 584-618.
[9] M.A. Teshager, S.D. Lin, B.J. Hwang, F.M. Wang, S. Hy, A.M. Haregewoin, ChemElectroChem, 3 (2016) 337-345.
[10] M. Egashira, H. Takahashi, S. Okada, J.-i. Yamaki, Journal of power sources, 92 (2001) 267-271.
[11] A.M. Haregewoin, A.S. Wotango, B.-J. Hwang, Energy & Environmental Science, 9 (2016) 1955-1988.
[12] J. Wang, Y. Yamada, K. Sodeyama, C.H. Chiang, Y. Tateyama, A. Yamada, Nature communications, 7 (2016) 12032.
[13] A. Tornheim, S. Sharifi-Asl, J.C. Garcia, J. Bareño, H. Iddir, R. Shahbazian-Yassar, Z. Zhang, Nano Energy, 55 (2019) 216-225.
[14] C.-C. Su, M. He, P.C. Redfern, L.A. Curtiss, I.A. Shkrob, Z. Zhang, Energy & Environmental Science, 10 (2017) 900-904.
[15] B. Flamme, M. Haddad, P. Phansavath, V. Ratovelomanana-Vidal, A. Chagnes, ChemElectroChem, 5 (2018) 2279-2287.
[16] C.C. Su, M. He, P. Redfern, L.A. Curtiss, C. Liao, L. Zhang, A.K. Burrell, Z. Zhang, ChemElectroChem, 3 (2016) 790-797.
[17] B. Gélinas, T. Bibienne, M. Dollé, D. Rochefort, Journal of Power Sources, 372 (2017) 212-220.
[18] H. Dong, Y. Zhang, S. Zhang, P. Tang, X. Xiao, M. Ma, H. Zhang, Y. Yin, D. Wang, S. Yang, ACS Omega, 4 (2019) 185-194.
[19] L. Xia, Y. Xia, C. Wang, H. Hu, S. Lee, Q. Yu, H. Chen, Z. Liu, ChemElectroChem, 2 (2015) 1707-1712.
[20] L. Xia, S. Lee, Y. Jiang, S. Li, Z. Liu, L. Yu, D. Hu, S. Wang, Y. Liu, G.Z. Chen, ChemElectroChem, 6 (2019) 3747-3755.
[21] G.B. Berhe, W.-N. Su, C.-J. Huang, T.M. Hagos, T.T. Hagos, H.K. Bezabh, M.A. Weret, L.H. Abrha, Y.-W. Yang, B.-J. Hwang, Journal of Power Sources, 434 (2019) 126641.
[22] C. Yang, L. Suo, O. Borodin, F. Wang, W. Sun, T. Gao, X. Fan, S. Hou, Z. Ma, K. Amine, K. Xu, C. Wang, Proc Natl Acad Sci U S A, 114 (2017) 6197-6202.

[23] V. Etacheri, O. Haik, Y. Goffer, G.A. Roberts, I.C. Stefan, R. Fasching, D. Aurbach, Langmuir, 28 (2011) 965-976.
[24] T.M. Hagos, G.B. Berhe, T.T. Hagos, H.K. Bezabh, L.H. Abrha, T.T. Beyene, C.-J. Huang, Y.-W. Yang, W.-N. Su, H. Dai, B.-J. Hwang, Electrochimica Acta, 316 (2019) 52-59.
[25] Y.-C. Yen, S.-C. Chao, H.-C. Wu, N.-L. Wu, Journal of The Electrochemical Society, 156 (2009) A95-A102.
[26] T.T. Hagos, B. Thirumalraj, C.J. Huang, L.H. Abrha, T.M. Hagos, G.B. Berhe, H.K. Bezabh, J. Cherng, S.F. Chiu, W.N. Su, B.J. Hwang, ACS Appl Mater Interfaces, 11 (2019) 9955-9963.
[27] V. Winkler, T. Hanemann, M. Bruns, Surface and Interface Analysis, 49 (2017) 361-369.
[28] J. Maibach, I. Källquist, M. Andersson, S. Urpelainen, K. Edström, H. Rensmo, H. Siegbahn, M. Hahlin, Nature communications, 10 (2019) 1-7.
[29] L. Cheng, S. Jandhyala, G. Mordi, A.T. Lucero, J. Huang, A. Azcatl, R. Addou, R.M. Wallace, L. Colombo, J. Kim, ACS applied materials & interfaces, 8 (2016) 5002-5008.
[30] H. Zheng, X. Zhou, S. Cheng, R. Xia, S. Nie, X. Liang, Y. Sun, H. Xiang, Journal of The Electrochemical Society, 166 (2019) A1456-A1462.